AGU PUBLICATIONS

JGR

Journal of Geophysical Research: Oceans

RESEARCH ARTICLE

10.1002/2016JC012585

Key Points:
- A new method is designed to detect the propagation route and speed of swells
- Propagation route and speed of the southern Indian Ocean westerly swells are revealed
- Propagation destination of the southern Indian Ocean westerly swells is presented

Correspondence to:
C. Y. Li,
lcy@lasg.iap.ac.cn

Citation:
Zheng, C. W., Li, C. Y., & Pan, J. (2018). Propagation route and speed of swell in the Indian Ocean. *Journal of Geophysical Research: Oceans*, *123*. https://doi.org/10.1002/2016JC012585

Received 24 NOV 2016
Accepted 27 NOV 2017
Accepted article online 6 DEC 2017

Propagation Route and Speed of Swell in the Indian Ocean

C. W. Zheng[1,2,3], C. Y. Li[1,4], and J. Pan[4]

[1]College of Meteorology and Oceanography, National University of Defense Technology, Nanjing, China, [2]State Key Laboratory of Estuarine and Coastal Research, Shanghai, China, [3]Navigation department, Dalian Naval Academy, Dalian, China, [4]State Key Laboratory of Numerical Modeling for Atmospheric Sciences and Geophysical Fluid Dynamics (LASG), Institute of Atmospheric Physics, the Chinese Academy of Sciences, Beijing, China

Abstract The characteristics of swell propagation play an important role in the forecasting of ocean waves as well as on research on global climate change, wave energy development, and disaster prevention and reduction. To reveal the propagation routes, terminal targets and speeds of swells that originate from the southern Indian Ocean westerly (SIOW), an intraseasonal swell index (SI) was defined based on the 45 year (September 1957 to August 2002) ERA-40 wave reanalysis data product from the European Center for Medium-Range Weather Forecasts (ECMWF). The results show that the main body of the SIOW-related swells typically spread to the waters off Sri Lanka and Christmas Island, while the branches spread to the Arabian Sea and other waters. The propagation speeds of swells originated in the SIOW were fastest in May and August, followed by November, and were slowest in February. Swells usually required 4–6 days to propagate from the western part of the SIOW to the waters off Sri Lanka and Christmas Island, whereas swells usually required 2–4 days to propagate from the eastern part of the SIOW to the waters off Christmas Island.

1. Introduction

Swells in the ocean can often be surprisingly destructive and lead to phenomena such as hogging and sagging, which can cause serious damage to ships. After being generated by a storm, waves can propagate very long distances with little attenuation until they break and dissipate upon reaching a coast (Alves, 2006; Ardhuin et al., 2009; Munk et al., 1963; Semedo, 2010; Snodgrass et al., 1966). These characteristics make swells an indicator of various atmospheric phenomena such as tropical cyclones, distant storms, or even large-scale sea breezes such as those related to monsoons. Swells also have significant impacts on the transport and dispersion of oil plumes within the ocean mixed layer, ocean surface roughness, wind stress, and other things (Chen et al., 2016; Hwang, 2008; Wu et al., 2016). Because of their substantial energy and good stability, energy production from swell waves has received increasing attention. Studies have shown that swells have a dominant status in a mixed wave (Semedo et al., 2011; Zheng et al., 2017), which means that swells also have a significant impact on air-sea interactions and global climate change. As a result, in-depth study of the characteristics of swells has practical value for swell wave power generation, ocean wave numerical simulation and forecasting, and studies of global climate change (Remya & Kumar, 2013; Remya et al., 2012).

Although data on swells are extremely scarce, previous researchers have provided important insights into swell generation and propagation. Arinaga and Cheung (2012) performed a global analysis of wind-sea and swells based on a 10 year simulation of wave data; their Figure 5 shows that the swell wave height (H^s) gradually decreases from south to north in each month and that contours have a northward salient. Zheng et al. (2014) analyzed the seasonal characteristics of the wave power densities of wind-sea, swells, and mixed waves; their Figure 2 shows that the Indian Ocean swell wave power density increases from west to east and tends to pile up to the west of Australia and then spreads to the north. Semedo (2010) noted that mixing of the global ocean by waves is dominated by swells; they also found that the winter swell in the North Atlantic Ocean displays north-south propagation. Semedo et al. (2011) presented the global seasonal characteristics of wind-sea, swells, and mixed waves, including wave direction and wave height. Zheng and Li (2017) contoured the wave direction and wave height of Indian Ocean swells based on the ERA-40 wave reanalysis and noted that the H^s contour has an obvious northward salient and that the dominant swell wave direction is south throughout the year. However, wave direction cannot indicate the long-distance route of swell movement. For example, in the low-latitude waters of the southern Indian Ocean, the swell wave direction is southeast, but this does not mean that the swell's propagation route in this region is from southeast to northwest. Alves (2006) noted that many southern Indian Ocean westerly (SIOW) swells freely propagate eastward into the tropical and subtropical latitudes of the Indian and Pacific Oceans. By monitoring the wave height and peak period, Remya et al. (2016) determined that swells propagated from the SIOW to northern Indian Ocean during 14–21 May 2005. By tracking the swell observations using SAR wave mode data, Jiang et al. (2016) found that swells generated by a storm in 58°S, 132°W could propagate to the coast of Mexico.

To date, studies of swell propagation routes, terminal targets, and propagation speeds have been relatively rare. In this study, the SIOW was divided into four regions. The swell index (SI) of each region was then defined to analyze the swell propagation characteristics, primarily their propagation routes, terminal targets, and propagation speeds, to provide a reference for ocean wave forecasting, energy development from swells, studies of air-sea interaction, and other applications.

2. Materials and Methods

2.1. Materials

The data set used in this study were the ERA-40 wave reanalysis from ECMWF, which is the first reanalysis product produced by coupling simulation results from a wave-atmosphere model (WAM) with assimilated observational data. Its range in space is 90°S–90°N and 180°W–180°E, its spatial resolution is 1.5° × 1.5°, and it covers the period from September 1957 to August 2002 at a time step of 6 h. The biggest advantage of this data set is that it separates wind-sea from swell waves. Because the ERA-40 wave reanalysis covers a long period and the entire global ocean, these data are widely used to analyze the character of global ocean waves, especially in the North Atlantic, North Pacific, and Southern Oceans (Caires et al., 2005; Hemer et al., 2007; Semedo et al., 2011). The ERA-40 wave reanalysis is divided into four different periods. However, problems in the observational data from December 1991 to May 1993 lead to the data assimilation time errors being relatively larger.

The criteria used for sea-swell separation is as follows (Semedo et al., 2009). The WAM model output is the two-dimensional wave energy spectrum $F(f, \theta)$ (Komen et al., 1994). Here, f is frequency and θ is direction. From these spectra, several derived integrated wave parameters can be obtained. The mean variance of the sea-surface elevation (the *zeroth* moment) is statistically related to the significant wave height: $SWH \cong H_s = 4.04\sqrt{m_0}$, where $m_0 = \int\int f^0 F(f,\theta) df d\theta$ is the variance or the zeroth moment. By weighting $F(f,\theta)$, θ_m is defined in the WAM mode as $\theta_m = a\tan(SF/CF)$, where the weights are defined as $SF = \int\int sin(\theta) F(f,\theta) df d\theta$ and $CF = \int\int cos(\theta) F(f,\theta) df d\theta$. The significant wave height, mean periods, and mean wave directions of wind-sea and swell waves are computed by separating the one-dimensional (1D) spectrum into wind-sea and swell components. The separation frequency is defined as the frequency corresponding to wave phase speed $\hat{c}$ where $33.6 \times (u_*/\hat{c}) \cos(\theta - \varphi) = 1$. The wind-sea and swell integrated parameters (in the present case m_0 and m_1) are computed by integrating over the respective 1-D spectral part.

Caires and Sterl (2005) validated the significant wave height (H_s) from ERA-40 against GEOSAT altimeter measurements from 1988, ERS-1 off-line (OPR) altimeter observations for June to December 1993, TOPEX altimeter measurements from 1993 onward, and ERS-2 OPR for June 1995 to May 1996. Using the method of Caires and Sterl (2005), the ERA-40 wave reanalysis data were validated against TOPEX/Poseidon altimeter swath measurements (available at http://www.aviso.altimetry.fr/en/data.html), as shown in Figure 1. The ERA-40 H_s and observed H_s were consistent during both JJA and DJF 2001. The correlation coefficient (CC), mean error (bias), root mean square error (RMSE), and scatter index (SI) were calculated to quantitatively analyze the accuracy of the ERA-40 H_s. There was an evident close relationship between ERA-40 H_s and observed H_s based on the results of CC, bias, RMSE, and SI. Additionally, Caires et al. (2004) determined that ERA-40 wave data are of better quality than similar wave reanalysis products. As a result, it can be concluded that ERA-40 wave reanalysis data are reliable in the Indian Ocean.

2.2. Methods

The SIOW was first divided into four regions as shown in Figure 2: A (40°–60°S, 40°–60°E), B (40°–60°S, 60°–80°E), C (40°–60°S, 80°–100°E), and D (40°–60°S, 100°–120°E). The propagation characteristics of swells that

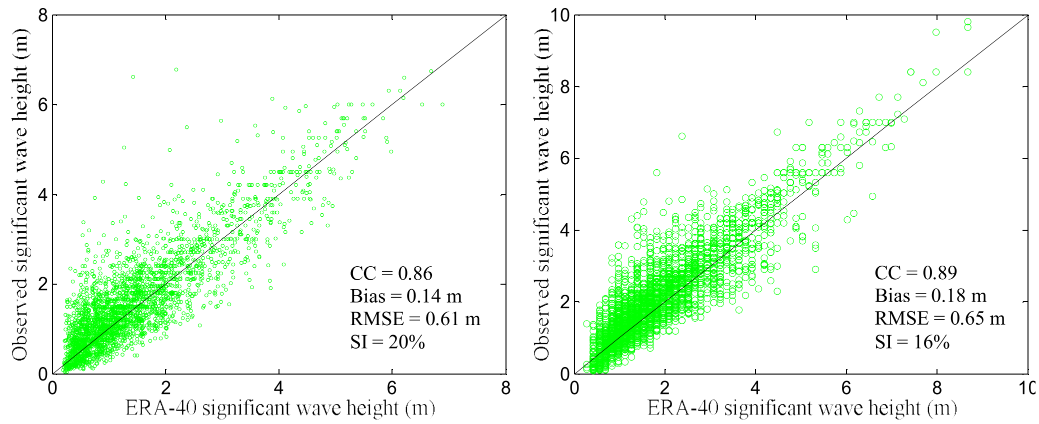

Figure 1. Correlation coefficients between ERA-40 significant wave height and observed significant wave height during (left) June–July–August (JJA) and (right) December–January–February (DJF) 2001.

originated in these four regions were then examined in the following analysis. Regions T1 (18°–28°S, 60°–80°E), T2 (10°–25°N, 80°–100°E), and T3 (10°–25°N, 55°–70°E) were randomly selected experimental areas chosen to determine if the SIOW-related swell could propagate to regions T1, T2, and T3. Regions E (10°S–10°N, 70°–90°E) and F (5°–25°S, 100°–120°E) were the key regions of swell propagation terminal targets. Then, the *SIs* of regions A, B, C, and D were calculated to analyze the characteristics of swell propagation. Calculation of the simultaneous, leading, and lagging correlations between *SI* and H^s in each 1.5° × 1.5° bin then revealed the propagation route, terminal target, and propagation speed.

The *SIs* were defined as follows. H^s in region A at 00:00 1 January 1958 was first regionally averaged to acquire the regional mean H^s, which represented the current swell index of region A (represented as SI_A). The 6 hourly SI_A values for the period between September 1957 and August 2002 were similarly obtained. Using the same method, values of SI_B, SI_C, and SI_D for the period between September 1957 and August 2002 were obtained at 6 h intervals.

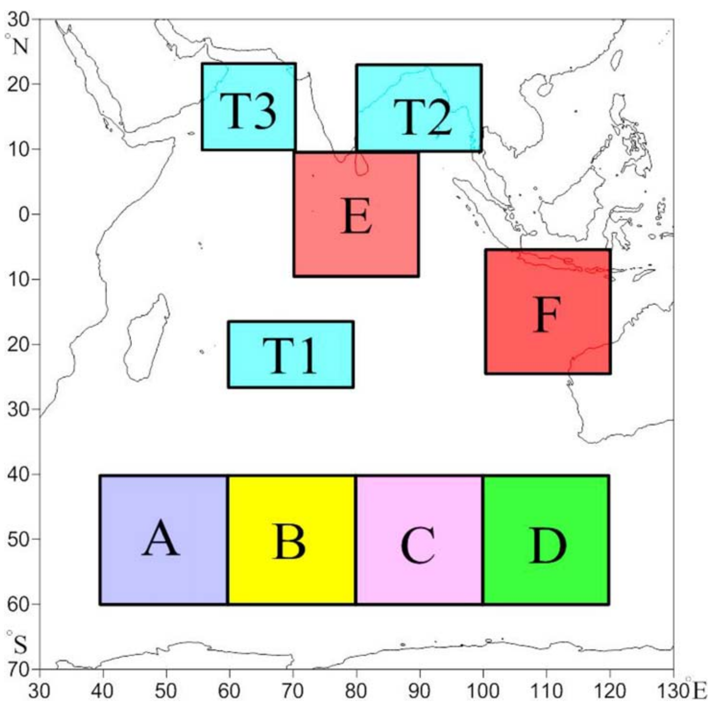

Figure 2. Geographical features of the Indian Ocean and the important regions in this study.

3. Results

3.1. Zonal Mean Characteristics

The 6 hourly values of sea surface wind speed (WS), wind sea wave height (H^w), and mixed wave height (H_s) for July 2001 and January 2002 were selected. A 6 hourly zonal average for each element was then calculated to exhibit the northward propagation phenomenon of each element, as shown in Figure 3.

The zonal mean characteristics of WS (not shown) were similar to those of H^w (Figures 3a and 3b). As shown in Figure 3a, the 0.5 m contour of H^w is clearly truncated in the equatorial region and near 40°S in January. As shown in Figure 3b, the 0.5 m contour of H^w is clearly truncated in the equatorial region and near 30°S in July. This result indicates that H^w could not propagate northward through the two obstacles. The zonal mean characteristics of H^s are shown in Figures 3c and 3d. Obviously, the 2.0 m contour of H^s in January exhibits an obvious northward propagation and southward shrinkage characteristic. Similar phenomenon can also be found in July through the 2.5 m contour of H^s. The zonal mean characteristics of H_s were similar to that of H^s, not shown here. Bhowmick et al. (2011) presented an overview of the swell in the Indian Ocean propagating from the Southern Ocean during the year 2005, as seen from WAM model simulations. Their results showed that the swells of the southern Indian Ocean can propagate across the equator. Our results

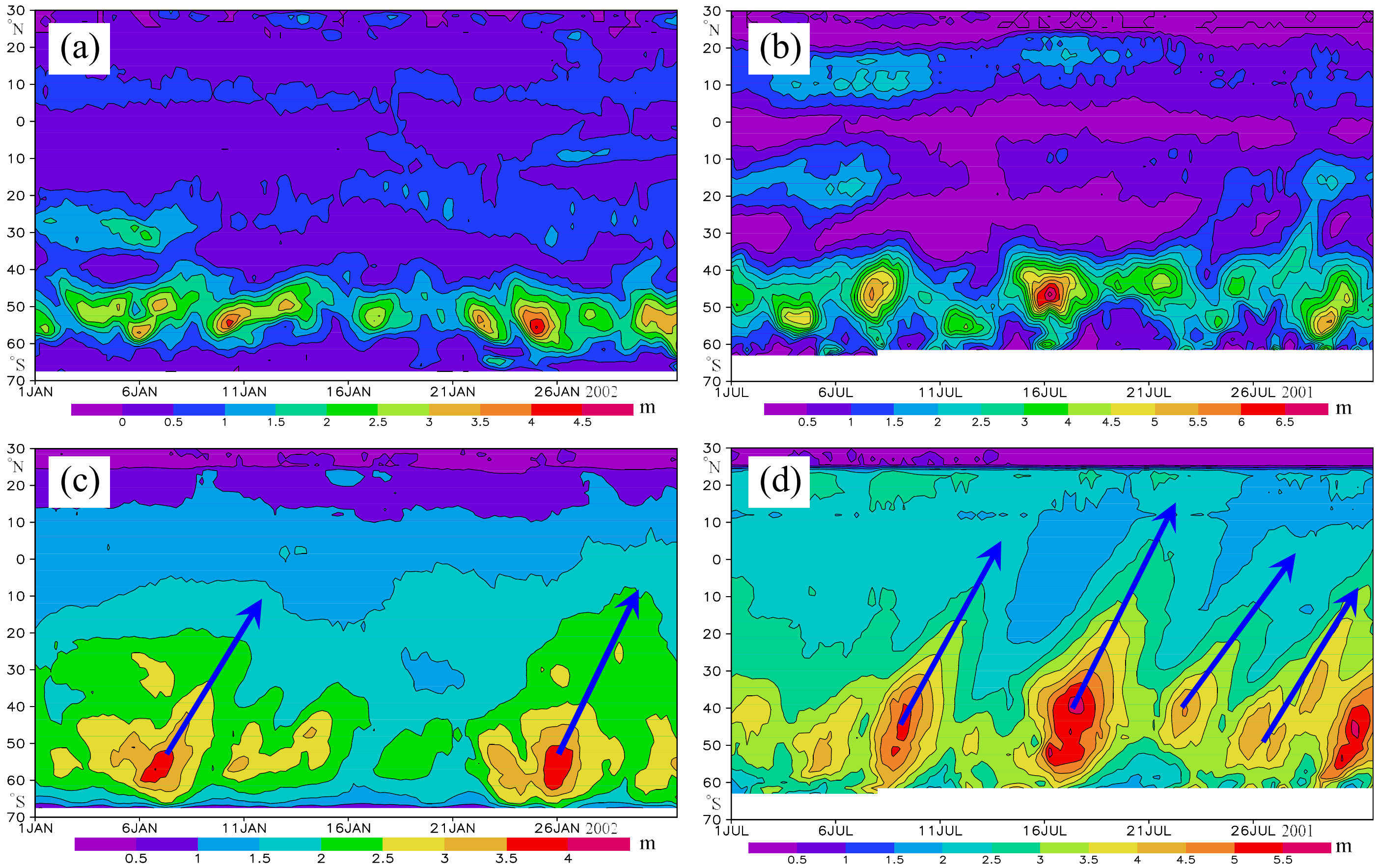

Figure 3. The 6 hourly zonal mean wave height of (a and b) wind-sea and (c and d) swell waves in (left) January 2002 and (right) July 2001. (a) Do zonal average of wind-sea wave height of the Indian Ocean at 00:00 1 January 2002 to obtain the current zonal mean value; 6 hourly zonal mean values of wind-sea wave height of the Indian Ocean in January 2002 were similarly obtained. The *x* axis is time, and the *y* axis is latitude. Using the same method of Figure 3a, the 6 hourly zonal mean values of (a and b) wind-sea wave height and (c and d) swell wave height of the Indian Ocean in January 2002 and July 2001 were obtained.

agreed well with those of Bhowmick et al. (2011). Moreover, swells even propagate beyond 10°N, as shown in Figure 2d. Just as the previous researchers pointed out, once generated, the swell wave can propagate very long distances with little attenuation until they break and dissipate upon reaching a coast (Alves, 2006; Munk et al., 1963; Semedo, 2010; Snodgrass et al., 1966). However, the wind-sea is quite different. According to the distribution of sea surface wind field (Figures omitted), it is not hard to find that the equator waters of the Indian Ocean is an obvious transition belt of wind direction from northeast monsoon to southeast trade wind in January, while it an obvious transition belt of wind direction from southwest monsoon to southeast trade wind in July. Similarly, near 40°S in January and near 30°S in July of the Indian Ocean are the transformation belts of wind direction from southeast trade wind to westerly. The significant variation of sea surface wind direction could disturb the wind-sea obviously.

3.2. Northward-Propagation Test of Swells

Figure 3 clearly shows the northward propagation of SIOW-related swells using 6 hourly data. Two experimental areas were randomly selected (regions T1, T2, and T3 in Figure 2) in this study for analysis to determine if SIOW-related swells could propagate to regions T1, T2, and T3. First, we selected a single JJA period (00:00 on 1 June 2001 through 18:00 on 31 August 2001); then, we drew 6 hourly curves of SI_A and H^s in region T1 (represented as H^S_{T1}), H^s in region T2 (represented as H^S_{T2}), and H^s in region T3 (represented as H^S_{T3}) to allow assessment of SI_A propagation to regions T1, T2, and T3. The results are shown in Figures 4–6.

As can be seen in Figure 4a, 6 hourly SI_A and H^S_{T1} did not show good simultaneous correlation, although there was an apparent lagging or leading correlation. Therefore, we quantitatively calculated the simultaneous, leading, and lagging correlations between the 6 hourly SI_A and H^S_{T1}, shown in Figure 4b. It is clear

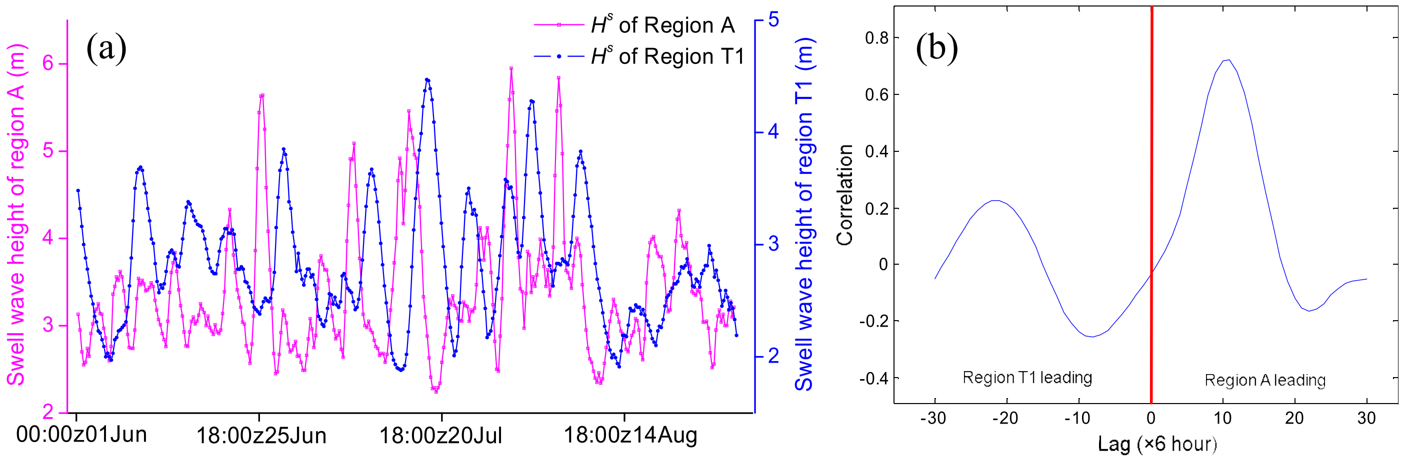

Figure 4. (a) 6 hourly H^s of regions A and T1 in JJA 2001 and (b) their simultaneous, leading, and lagging correlation coefficients.

that the simultaneous correlation was very poor; the correlation coefficient (R) was close to 0. When a lag of 10 intervals (60 h) relative to H^S_{T1} was used, the R reached its peak value of 0.7, which is significant at the 0.001 level. To display the strong lagged correlation more clearly, curves of H^S_{T1} using a 10 interval lag and SI_A are shown in Figure 5. The curves in Figure 5 show a high degree of similarity, which means that swells that originated in region A could propagate to region T1 (Madagascar waters) in JJA. It is obvious from Figures 6a and 6b that the simultaneous, leading, and lagging correlations between SI_A and H^S_{T2} were very poor, within ± 0.2, which means that swells that originated in region A did not propagate to region T2, which is in the central-north part of the Bay of Bengal. Similarly, as shown in Figures 6c and 6d, swells that originated in region A did not propagate to region T3 in this experiment, which is in the top of the Arabian Sea.

3.3. Main Propagation Routes of Swells

We found through the preceding analyses (Figures 4–6) that swells that originated in region A clearly propagated northward. We calculated the simultaneous, leading, and lagging correlations between 6 hourly SI_A and H^s in each 1.5° × 1.5° grid cell. Similarly, the correlations between 6 hourly SI_B and H^s, SI_C and H^s, and SI_D and H^s were calculated in each 1.5° × 1.5° grid cell.

3.3.1. Exploration of Main Propagation Routes

We selected a single JJA period (00:00 on 1 June 2001 through 18:00 on 31 August 2001) and then calculated the simultaneous, leading, and lagging correlations between 6 hourly SI_A and H^s in each 1.5° × 1.5° grid cell to find the main propagation route of swells that originated in region A. The leading correlation of H^s was not significant (not shown). The correlation coefficients between 6 hourly SI_A and simultaneous H^s in

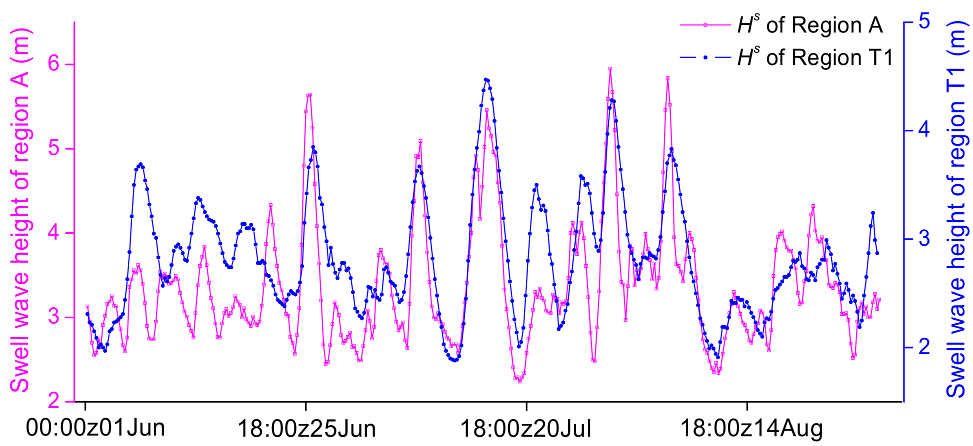

Figure 5. 6 hourly H^s of region A and H^s of region T1 (lagged by 10 intervals) in JJA 2001.

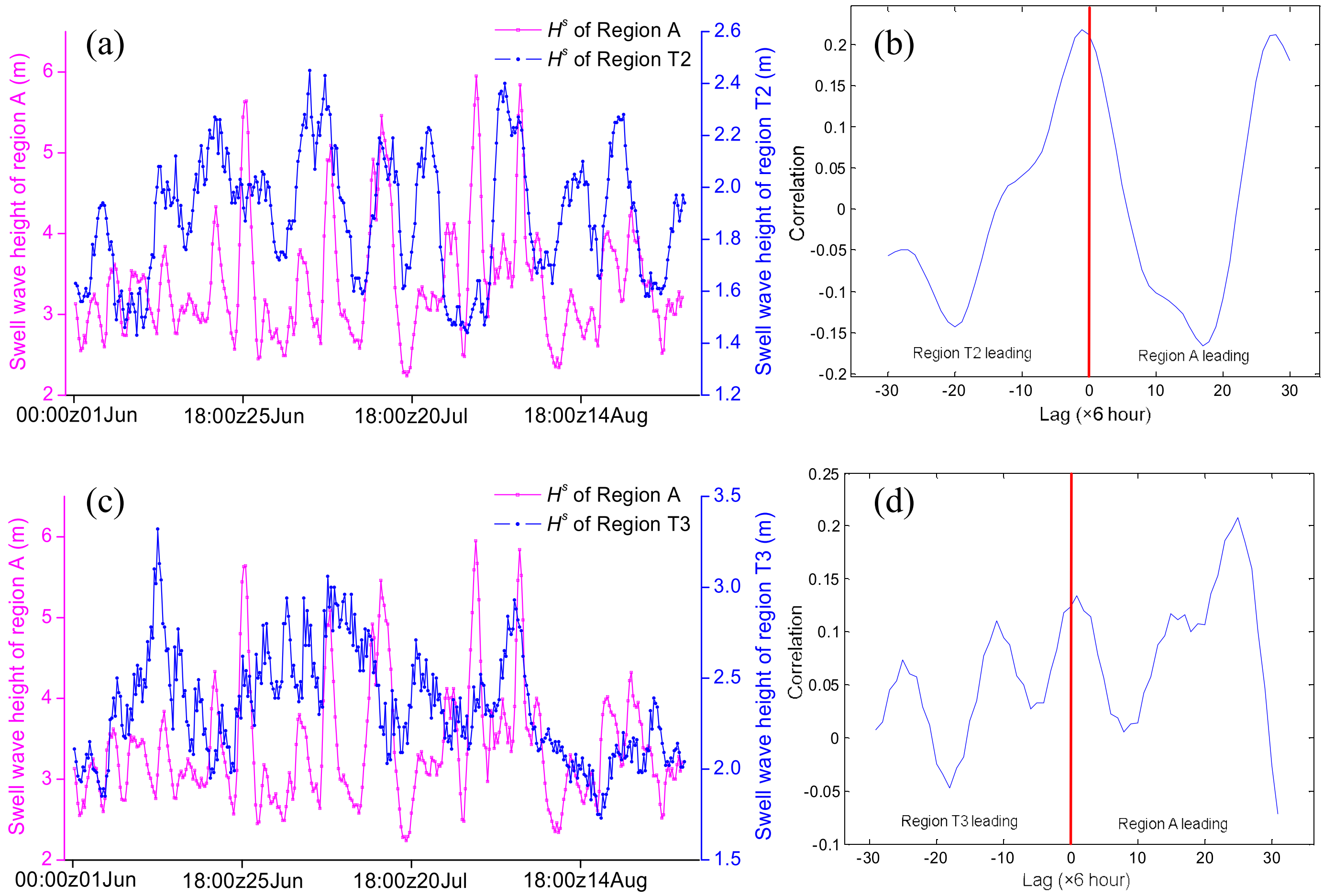

Figure 6. 6 hourly H^s of (a) regions A and T2 and (b) region A and T3 in JJA 2001 and (b and d) their simultaneous, leading, and lagging correlation coefficients separately.

each 1.5° × 1.5° grid cell in JJA 2001 were calculated and are shown in Figure 7a. The correlation coefficients between the 6 hourly values of H^s (lagged by 48, 96, 120, 144, and 168 h) and SI_A in JJA 2001 were calculated for each 1.5° × 1.5° grid cell and are shown in Figures 7b–7f.

The values of H^s in an approximately circular area near region A show good simultaneous correlation with SI_A (the areas that passed the 0.001 significant reliability level are colored) and are above 0.8 in the large center. After 21 h (i.e., with H^s lagged by 24 h), the shape of the region that was significant at the 0.001 reliability level changed from approximately circular to the northwest-southeast direction. During the process of propagation, the area that passed the significance threshold expanded, and the value of the CC diminished, which means that the swells that originated in region A gradually became diffuse and decreased during the propagation process. From 0 to 24 h, the large area of high CC moved northeast to Kerguelen Island. From 24 to 48 h, the large area continued to move northeast to the east of Madagascar. By 48 h, the swell had propagated northeast to the Bay of Bengal. The area that passed the significance threshold gradually shrank and the CC value decreased during the propagation process. By 168 h, the swell had propagated to the middle of the Bay of Bengal. Note that 120 h later, one of the branches had spread to the waters between the island of Java and Australia. As a result, it is not hard to find that the main body of the SIOW-related swells spread to the Sri Lanka waters, while partial of the SIOW-related swells can also spread to the south of the Arabian Sea and other waters.

By using the observations, Remya et al. (2016) found 10 high swell events in North Indian Ocean (NIO) (also named Kallakkadal events) during 2005, which are caused by the swells propagating from south of 30°S. In all cases, 3–5 days prior to the high swell events in NIO, they observed a severe low pressure system, called

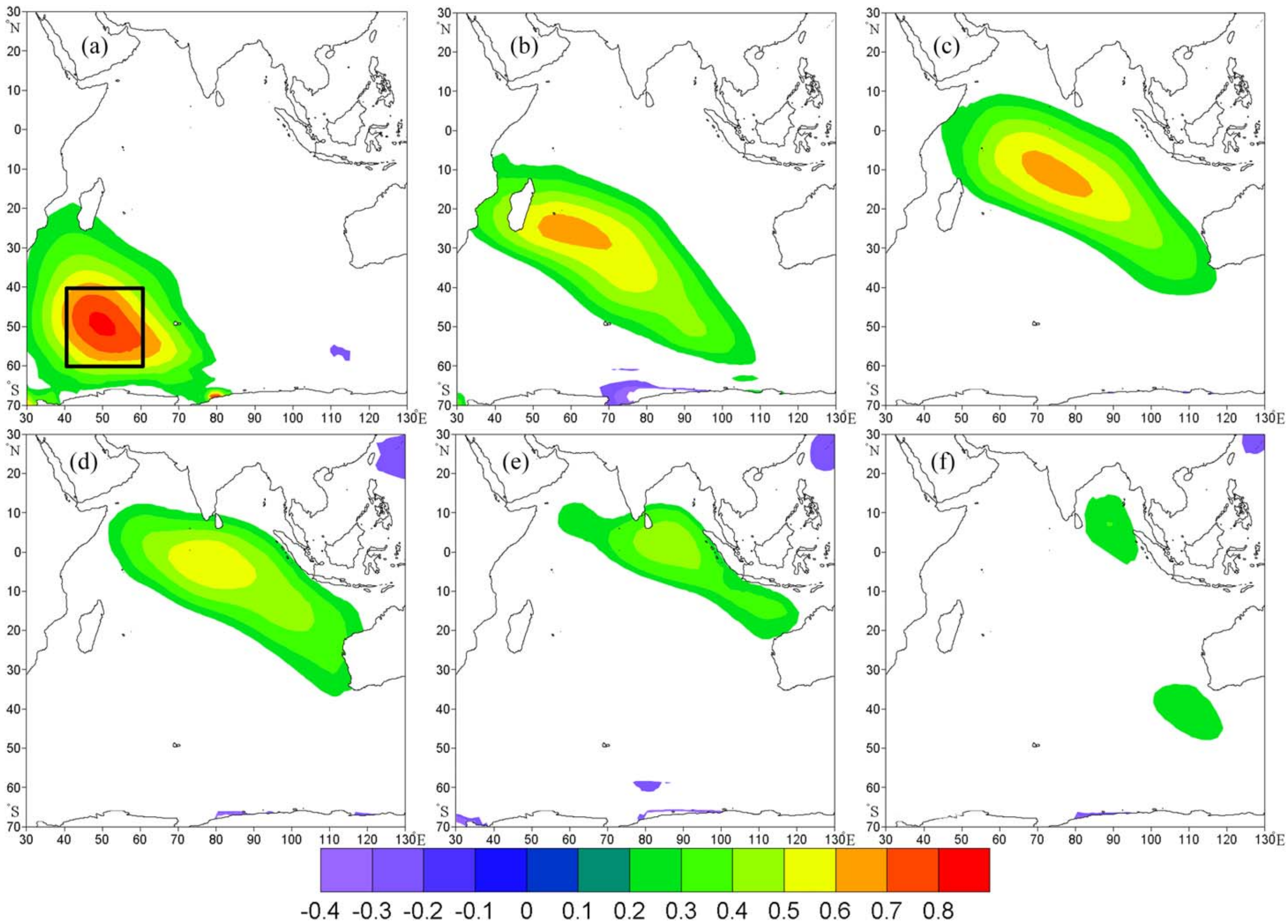

Figure 7. The calculated and contoured correlations between 6 hourly SI_A and H^s for each 1.5° × 1.5° bin in JJA 2001. (a) The correlation coefficients (CC) between 6 hourly SI_A and simultaneous H^s at each 1.5° × 1.5° bin in JJA 2001. (b) The CC between the 6 hourly values of H^s at each 1.5° × 1.5° bin for a lag of 48 h and SI_A in JJA 2001. (c, d, e, and f) The CC between the 6 hourly values of H^s at each 1.5° × 1.5° bin for separate lags of 96, 120, 144, and 168 h and SI_A in JJA 2001. In this figure, only the areas significant at a 0.001 reliability level are colored.

the Cut-Off Low (COL) in the Southern Ocean. These COLs provides strong (about 25 m/s) and long duration (about 3 days) surface winds over a large fetch; essential conditions for the generation of long-period swells. The intense equator ward winds associated with COLs in the Southern Indian Ocean (SIO) trigger the generation of high waves, which propagate to NIO as swells. Furthermore, these swells cause high wave activity and sometimes Kallakkadal events along the NIO coastal regions. The overall propagation characteristic of SIOW-related swells in this study is agreed with Remya et al. (2016).

3.3.2. Propagation Route in JJA and DJF

Figure 7 roughly shows the propagation of swells that originated in region A in JJA but does not show a clear route. To display the propagation route more clearly, the relatively large areas in each plot of Figure 7 were first highlighted and then connected with a single line, as shown in Figure 8a, where the red arrow represents the main propagation route. Similarly, the propagation routes of swells that originated in regions A, B, C, and D in JJA and DJF are presented in Figure 8.

3.3.3. JJA

Swells that originated in region A mainly spread to the east of Sri Lanka (Sri Lanka waters) in a north-northeasterly direction and gradually became diffuse and diminished during the propagation process. Swells that originated in region B first propagated north-northeast for a short distance. At 40°S, the propagation direction turned to the north, and at 10°S, the propagation direction turned to the northeast; the propagation target was near Sri Lanka. Swells that originated in region C mainly spread to 105°E in an east-

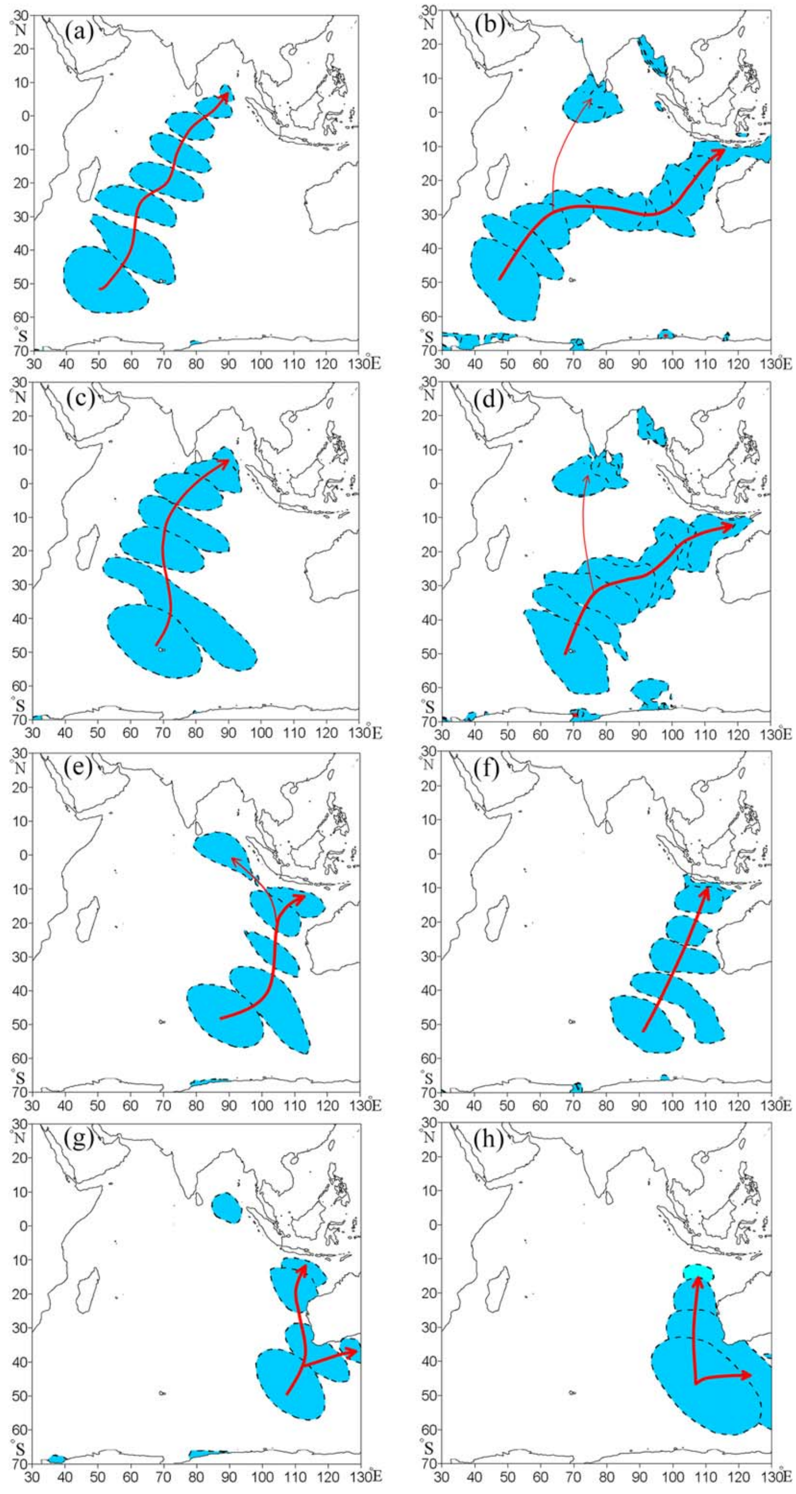

Figure 8. Main propagation routes of swells that originated in regions (a and b) A, (c and d) B, (e and f) C, and (g and h) D in (left) JJA 2001 and (right) DJF 2001. (a) The correlation coefficients (CC) between 6 hourly SI_A and simultaneous H^s at each 1.5° × 1.5° bin in JJA 2001 were calculated and contoured. Then, the relative large value of CC $\geq$ 0.5 was contoured with the dotted line as the edge and filled with blue color. The CC between H^s of separate 24, 48, 72, 96, 120, and 144 h lags with SI_A were similarly calculated. Then, the relative large values of CC $\geq$ 0.5 were also separately contoured with the dotted line as the edge and filled with blue color. The relatively large values of CC were connected by the red solid line. The swell propagation routes in region A were thus obtained. The arrow represents the propagation direction. (b–h) The same method used in (a) was used to plot the swell propagation routes in regions B, C, and D in JJA and DJF.

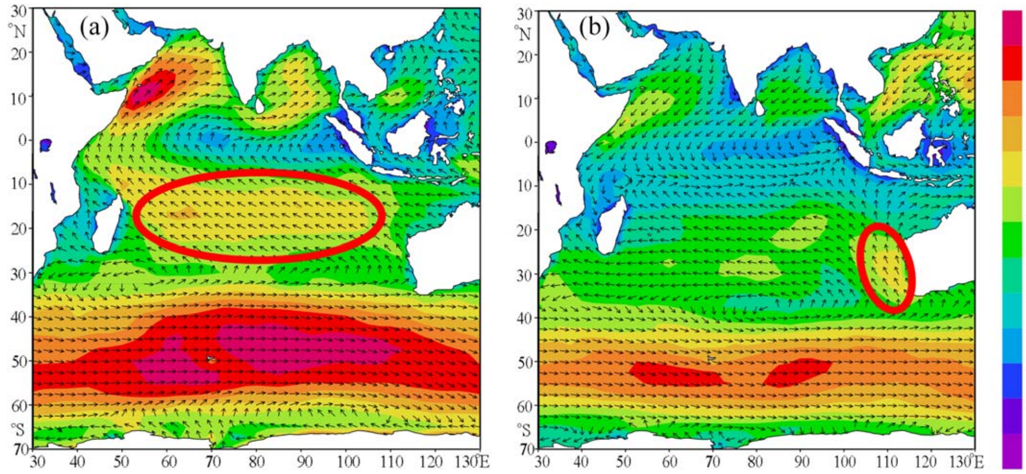

Figure 9. Sea surface wind field in (a) JJA 2001 and (b) DJF 2001. Colors represent wind speed (m/s) and unit arrows represent wind direction.

northeasterly direction for the first 24 h. Then, the main body of the swells moved northward along the western coast of Australia because of terrain effects. At 20°S, one branch spread in a northeasterly direction to the waters between the island of Java and Australia (the waters off Christmas Island), and another branch spread along the south coast of Sumatra to the waters east of Sri Lanka. Swells that originated in region D mainly spread in a northeasterly direction for the first 24 h. The swells were cut into two parts by land when they reached the southwest corner of Australia; one branch moved to the east along the south coast of Australia, whereas the other branch moved northward to the waters between the island of Java and Australia.

Comparison of the four routes in JJA (Figure 8, left) clearly shows that the propagation routes of swells that originated in regions C and D in JJA were significantly affected by the Australian landmass. The corresponding sea surface wind field in JJA 2001 is also presented in Figure 9a. Combined with Figures 8a and 8c and 9a, it is clear that the sea surface wind field plays an important leading role in determining the propagation routes of swells that originate in regions A and B. One important region is the southeast trade wind zone in the low latitudes of the southern Indian Ocean (shown by the red solid line in Figure 9a). Relatively strong southeast trade winds, which have an average wind speed of 7–10 m/s, caused the first change in swell propagation direction (from northeast to north) to pass through the equator. When spreading to Madagascar's northeastern coast, the strong southwest monsoon in the northern Indian Ocean had a significant effect on the propagation direction of swells and caused the direction of propagation to change from north to northeast.

3.3.4. DJF

Swells that originated in region A mainly spread in a north-northeasterly direction to 30°S, where they abruptly turned to the east-southeast. The propagation direction strongly changed again, to the northeast, when they spread to 100°E. The main body of the swells spread to the waters off Christmas Island 192 h later. The propagation route of swells that originated in region B was relatively simple; they propagated northeast and spread to the waters off Christmas Island approximately 144 h later. The propagation route of swells that originated in region C was also simple; they propagated north-northeast and spread approximately 120 h later to the waters off Christmas Island. Swells from region D were cut into two parts by land when they spread to the southwest corner of Australia; one branch moved to the east along the south coast of Australia, and the other branch moved northward to the waters off Christmas Island.

Comparing the four routes seen in DJF (Figure 8 right), it is clear that the propagation routes of swells that originated in regions A and B were different from those in JJA. Combined with the sea surface wind field (Figure 9b) and propagation route, it is clear that the southeast trade winds of the low-latitude southern Indian Ocean in DJF are not as strong as those in JJA, with the result that the southeast trade wind cannot lead the main body of swells from the west region of the SIOW to cross the equator. Additionally, the frequent inputs of cold air from the northern Indian Ocean may suppress the northward swell propagation. Note that the relatively large area of high wind speeds west of Australia (shown by the red solid line in

Figure 9b) may play a positive role in the northward propagation of swells in the eastern region of the SIOW. The propagation route of swells from region D is significantly affected by the terrain of Australia.

Samiksha et al. (2012) found that a series of very high swells that originated at 40°S, off the southern tip of South Africa, propagated to the northeast and broke over the island of Reunion in the subtropical waters of the southern Indian Ocean. A similar phenomenon was also reported by Alves (2006). Our results agree with those of Samiksha et al. (2012) and Alves (2006), although the northward propagation is more obvious in our analysis. Aboobacker et al. (2011) and Glejin et al. (2013) determined that the predominant northward swell propagation (coming from the south) in the midwest of the Arabian Sea is disrupted during DJF and that the Shamal swells play an important role in this disruption. Similarly, the swells and wind-seas generated by the cold airs in DJF in the northern Indian Ocean may have disrupted the northward propagation of the swells. The southern hemisphere is winter in JJA, and the strength of SIOW wind speed in summer is weaker than that in winter. The above two phenomena determined that the swell in the west of the SIOW in DJF could not propagate northward as far as that in JJA.

3.4. Swell Propagation Speed and Terminal Target

It can clearly be seen in Figure 8 that swells that originated in regions A, B, C, and D in JJA and DJF often propagated to two areas: the waters off Sri Lanka (region E in Figure 2) and Christmas Island (region F in Figure 2; the waters between the island of Java and Australia). The multiyear average CCs from January to December between swells of the above regions were calculated; only the CCs between regions C and F are presented in Figure 10.

SI_C clearly plays a leading role in each month. The correlation coefficient (CC) usually reaches the peak value and SI_C leads by 10–20 intervals (60–120 h). July was selected as an example to analyze the speed of swell propagation. In July, the CC reached its peak value of 0.53 (significant at the 0.001 level) when SI_C led by 14 intervals (84 h). This result means that the propagation of swells from region C to region E required approximately 84 h. The swell propagation speed from region C to region E in each month could be obtained in the same way.

Using the method shown in Figure 10, the multiyear average leading and lagging correlations from January to December between 6 hourly SI_A and H_E^S, SI_B and H_E^S, SI_C and H_E^S, SI_D and H_E^S, SI_A and H_F^S, SI_B and H_F^S, SI_C and H_F^S, and SI_D and H_F^S were calculated. Then, the seasonal characteristics of the above correlations were analyzed as shown in Table 1, with February, May, August, and November selected as the representative months for DJF, March–April–May (MAM), JJA, and September–October–November (SON), respectively.

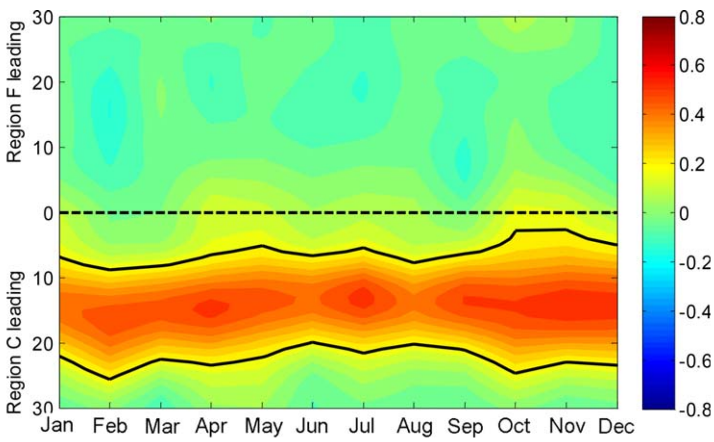

Figure 10. Monthly characteristics of leading and lagging correlations between swells in regions C and F. First, the CCs between 6 hourly SI_C and H_F^S in September 1957 were calculated, including leads and lags of 30 intervals. Using the same method, the monthly correlations between 6 hourly SI_C and H_F^S for the 540 months between September 1957 and August 2002 were obtained. Then, the multiyear average CCs from January to December were obtained. The area in the black solid line is significant at the 0.05 reliability level.

3.4.1. Propagation Speed of Swells That Originated in Region A

The CCs between SI_A and lagged H_E^S were best for February (0.55) and November (0.50), followed by May (0.42), and were smallest in August (0.38). The CCs between SI_A and H_E^S usually reached their peak value when H_E^S was lagged by 22–24 intervals (132–144 h). This result means that the propagation of swells from region A to region E required 132–144 h. The CCs between H_F^S and SI_A were much smaller than those between H_E^S and SI_A for each month. The propagation of swells from region A to region F required 27 intervals (162 h) in February and 23–24 intervals (138–144 h) in

Table 1
Correlation Coefficients (CCs) Between Swells in Regions A/B/C/D and Regions E/F (Arrows (→) Indicate Swell Propagation from Regions A/B/C/D to E/F; Figures Without Underlining Indicate Significance at the 0.001 Level; Figures With Underlining Are not Statistically Significant)

Swells' propagation direction	February		May		August		November	
	CC	Lagging intervals of E/F (×6 h)	CC	Lagging intervals of E/F (×6 h)	CC	Lagging intervals of E/F (×6 h)	CC	Lagging intervals of E/F (×6 h)
A→E	0.55	24	0.42	22	0.38	22	0.50	23
A→F	0.30	27	0.31	23	0.26	23	0.36	24
B→E	0.59	20	0.43	18	0.40	18	0.54	19
B→F	0.39	22	0.42	18	0.35	18	0.46	19
C→E	0.47	15	0.32	14	0.33	14	0.47	14
C→F	0.48	17	0.47	13	0.41	14	0.54	15
D→E	0.34	10	0.17	7	0.24	8	0.34	7
D→F	0.47	12	0.43	9	0.38	9	0.52	9

May, August, and November, which means that the speed of swell propagation from region A to region F in February was much slower than in other months.

3.4.2. Propagation Speed of Swells That Originated in Region B

The propagation speed and terminal target of swells that originated in region B were similar to those of swells that originated in region A. Additionally, they usually required 4–5 more intervals (24–30 h) to propagate from region A to regions E and F.

3.4.3. Propagation Speed of Swells That Originated in Region C

The CCs between H_{F}^{S} and SI_C were much greater than the CCs between H_{E}^{S} and SI_C for each month, which means that the swells that originated in region C mainly propagated to the waters off Christmas Island, although a small branch could spread to the waters off Sri Lanka. The propagation of swells from region C to region E or F usually required 13–15 intervals (78–90 h).

3.4.4. Propagation Speed of Swells That Originated in Region D

The CCs between H_{F}^{S} and SI_D were much greater than those between H_{E}^{S} and SI_D for each month, which means that swells that originated in region D mainly propagated to the waters off Christmas Island. It is worth noting that CCs between H_{E}^{S} and SI_D in February, August, and November were also significant at the 0.05 level. Combining this result with Figures 8g and 8h, we found that swells that originated in region D did not generally spread to Sri Lanka waters, although the correlation between $\mathrm{SI_D}$ and H^s in a small region near Sri Lanka passed the significance threshold. This result occurred because region D and regions A, B, and C are all located in the SIOW, which produced similar H^s values in these four regions. Moreover, the H^s values of regions A, B, and C could spread to region E, which would cause swells from region E to have the features of regions A, B, and C. Finally, although swells that originated in regions D and E appeared to have some correlation with one another, no significant propagation from region D to region E occurred.

Overall, the propagation of swells from SIOW to region E and F usually required 3–6 days. Remya et al. (2016) found that 10 high swell events in North Indian Ocean (NIO) (also named Kallakkadal events) during 2005 are caused by the swells propagating from south of 30°S. In all cases, 3–5 days prior to the high swell events in NIO. Nayak et al. (2013) found that the low-frequency swells from the Southern Ocean reach the southern tip of Indian mainland in about 4 days without much energy dissipation. Our results agreed well with those of Remya et al. (2016). In addition, the propagation speed of swells in the Indian Ocean was fastest (required the shortest time) in May and August, followed by November. It was slowest (required the longest time) in February. This result occurred because DJF in the southern Indian Ocean corresponds to summer, whereas JJA corresponds to winter. The intensity of westerly winds in winter was obviously stronger than that in summer, which resulted in a faster swell propagation speed in JJA. Remya et al. (2016) have provided important insights into the SIO meteorological conditions prior to the NIO high wave events. They pointed out that the strong equator ward surface winds associated with COL development. These strong and persistent winds generated high waves at the COL active region. The strong south south-westerly surface wind fields associated with the COL, generated waves that propagate toward north north-east into the NIO in a band of frequencies with a peak wave period of around 20 s. And in all cases, 3–5 days prior to the high swell events in NIO, they observed a severe low pressure system, called the COL in the Southern Ocean.

Zheng and Li (2017) analyzed the interannual and interdecadal variabilities and intraseasonal oscillations of WS, H^w, H^s, and H_s in the Roaring Forties and tropical waters of the Indian Ocean. Their results show that the WS and H^s in the Roaring Forties and H^s in the tropical waters of the Indian Ocean share a common period of approximately 8 days (weekly oscillation) on an intraseasonal scale. And approximately 132–138 h are required for H^s to propagate from the Roaring Forties to the tropical waters of the NIO. Based on the results from Remya et al. (2016) and Zheng and Li (2017), it means that the natural hazards along the NIO coasts can be forecasted at least 2 days in advance if the meteorological conditions of the SIO are properly monitored.

Note that the CCs in Table 1 were usually largest in February and November and smallest in August, although the Southern Hemisphere westerlies are stronger in August than in February and November. The southwest monsoon in the northern Indian Ocean is also very strong in this season. Swells generated by the strong southwest monsoon can also affect the waters off Sri Lanka. As a result, JJA swells in the waters off Sri Lanka had the signals of swells from both the SIOW and the southwest monsoon, which resulted in a weaker relationship between swells of different regions in August. The Southern Hemisphere westerlies in February and November are weak because it is summer, which does not promote the long-distance northward propagation of swells as in August. The wind-seas and swells generated by cold air from the northern Indian Ocean may have disrupted the northward propagation of the swell. However, the intensity of cold air was much weaker than the southwest monsoon in JJA, which meant less impact on the northward swell propagation. As a result, the CCs between swells of different regions in February and November were greater than in August.

3.4.5. Propagation Terminal Target

Examination of Figure 8 and Table 1 clearly shows that most SIOW-related swells in DJF mainly propagated to the waters off Christmas Island. Moreover, a small portion of swells that originated in the west of the SIOW (regions A and B) could spread to Sri Lanka waters. In JJA, swells that originated in the west of the SIOW mainly propagated to Sri Lanka waters, whereas swells that originated in the east of the SIOW (regions C and D) mainly propagated to the waters off Christmas Island.

Combining Figure 8 and Table 1, it is clear that there was a close relationship among swells in the SIOW and the waters off Sri Lanka and Christmas Island. To directly display this close relationship, we contoured the values of SI_A, SI_B, SI_C, SI_D, and lagged H^S_F in DJF 2001 (this period was selected at random; similar phenomena

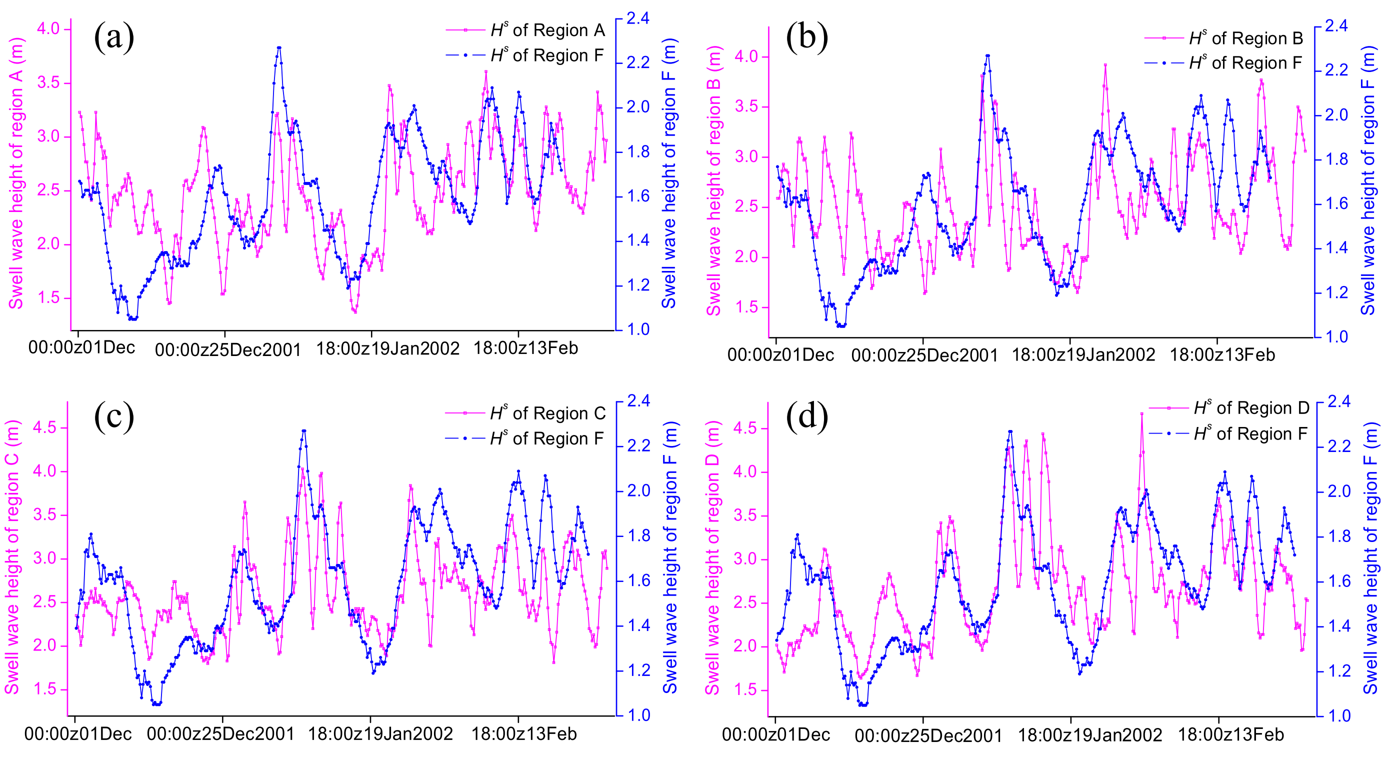

Figure 11. 6 hourly H^s of regions A, B, C, and D and lagged H^s of regions F in DJF 2001.

can also be found in other time periods), as shown in Figure 11. Obviously, the curves in Figure 11 are quite consistent. This result again shows that swells from the SIOW can propagate to the waters off Christmas Island.

4. Conclusion and Prospects

The propagation routes, terminal targets, and propagation speeds of SIOW-related swells were analyzed based on the ERA-40 wave reanalysis from ECMWF. The results were as follows:

The main body of the SIOW-related swells mainly spread to two regions, the waters off Sri Lanka and Christmas Island, while the branches spread to the Arabian Sea and other waters. In JJA, swells from the western part of the SIOW (40°–80°E) usually propagated to the waters off Sri Lanka, whereas swells from the east region (80°–120°E) usually propagated to the waters off Christmas Island. In DJF, swells from the entire region of the SIOW mainly propagated to the waters off Christmas Island.

The Australian landmass had a significant impact on swell propagation routes in the eastern region of the SIOW. When spreading to the southwest corner of Australia, swells were cut into two parts by the land; one branch moved to the east along the southern coast of Australia, whereas the other branch moved northward to the waters off Christmas Island.

The sea surface wind field had an obvious leading or inhibitory effect on swell propagation. The southeast trade winds in the low-latitude southern Indian Ocean had an important leading role in the propagation route of swells in the middle and western regions of the SIOW, especially in JJA. Relatively strong southerly winds in the west of Australia played a positive role in the northward propagation of swells, especially in DJF. The wind-sea and swell generated by the cold air of the northern Indian Ocean disrupted the northward propagation of the swell in DJF.

The swell propagation speed in the Indian Ocean was fastest in May and August, followed by November, and was slowest in February. Swell usually required 132–144 h to propagate from region A to regions E or F, 108–132 h to propagate from region B to regions E or F, 78–90 h to propagate from region C to E/F, and 54 h to propagate from region D to region F.

The relationships between swells in the SIOW and the waters off Sri Lanka, as well as those between swells in the SIOW and the waters off Christmas Island, were usually best in February and November, followed by May, and were smallest in August.

This study presented a method to exhibit the propagation route of swells, and JJA 2001 and DJF 2001 were taken as a case study. In the future actual application, it is necessary to present the propagation features of swells in each month, thus to establish a practical reference for swell wave power generation, ocean wave forecasting, research on global climate change, and other applications.

Acknowledgments
This work was supported by the Open Research Fund of State Key Laboratory of Estuarine and Coastal Research (grant SKLEC-KF201707), the Nature Science Foundation of China (41490642 and 41775165), the National Basic Research Program of China (2013CB956203 and 2015CB453200), the Key Laboratory of Renewable Energy, Chinese Academy of Sciences (Y707k31001), and the Junior Fellowships for CAST Advanced Innovation Think-tank Program (DXB-ZKQN-2016-019). All the authors would like to thank anonymous referees and the editor for providing their excellent comments and valuable advice for improving this paper. All the authors would like to thank ECMWF for providing the ERA-40 wave reanalysis (Available at http://apps.ecmwf.int/datasets/data/era40-daily/levtype=sfc/).

References

Aboobacker, V. M., Vethamony, P., & Rashmi, R. (2011). Shamal" swells in the Arabian Sea and their influence along the west coast of India. *Geophysical Research Letters*, *38*, L03608. https://doi.org/10.1029/2010GL045736

Alves, J. H. (2006). Numerical modeling of ocean swell contributions to the global wind-wave climate. *Ocean Modelling*, *11*, 98–122.

Ardhuin, F., Chapron, B., & Collard, F. (2009). Observation of swell dissipation across oceans. *Geophysical Research Letters*, *36*, L06607. https://doi.org/10.1029/2008GL037030

Arinaga, R. A., & Cheung, K. F. (2012). Atlas of global wave energy from 10 years of reanalysis and hindcast data. *Renewable Energy*, *39*, 49–64.

Bhowmick, S. A., Kumar, R., Chaudhuri, S., & Sarkar, A. (2011). Swell propagation over Indian Ocean Region. *International Journal of Ocean and Climate Systems*, *2*(2), 87–99.

Caires, S., & Sterl, A. (2005). Validation and non-parametric correction of significant wave height data from the ERA-40 reanalysis. *Journal of Atmospheric and Oceanic Technology*, *22*, 443–459.

Caires, S., Sterl, A., Bidlot, J. R., Graham, N., & Swail, V. (2004). Intercomparison of different wind wave re-analyses. *Journal of Climate*, *17*(10), 1893–1913.

Caires, S., Sterl, A., & Gommenginger, C. P. (2005). Global ocean mean wave period data: Validation and description. *Journal of Geophysical Research*, *110*, C02003. https://doi.org/10.1029/2004JC002631

Chen, B., Yang, D., Meneveau, C., & Chamecki, M. (2016). Effects of swell on transport and dispersion of oil plumes within the ocean mixed layer. *Journal of Geophysical Research: Oceans*, *121*, 3564–3578. https://doi.org/10.1002/2015JC011380

Glejin, J., Kumar, V. S., Nair, T. M. B., Singh, J., & Mehra, P. (2013). Observational evidence of summer Shamal swells along the west coast of India. *Journal of Atmospheric and Oceanic Technology*, *30*, 379–388.

Hemer, M. A., Church, J. A., & Hunter, J. R. (2007). Waves and climate change on the Australian coast. *Journal of Coastal Research*, *50*, 432–437.

Hwang, P. A. (2008). Observations of swell influence on ocean surface roughness. *Journal of Geophysical Research*, *113*, C12024. https://doi.org/10.1029/2008JC005075

Jiang, H., Stopa, J. E., Wang, H., Husson, R., Mouche, A., Chapron, B., & Chen, G. (2016). Tracking the attenuation and nonbreaking dissipation of swells using altimeters. *Journal of Geophysical Research: Oceans*, *121*, 1446–1458. https://doi.org/10.1002/2015JC011536

Komen, G. J., Cavaleri, L., Doneland, M., Hasselmann, K., Hasselmann, S., & Janssen, P. A. E. M. (Eds.). (1994). *Dynamics and modelling of ocean waves*. Cambridge, UK: Cambridge University Press.

Munk, W. H., Miller, G. R., Snodgrass, F. E., & Barber, N. F. (1963). Directional recording of swell from distant storms. *Philosophical Transactions of the Royal Society London*, *A255*, 505–584.

Nayak, S., Bhaskaran, P. K., Venkatesan, R., & Dasgupta, S. (2013). Modulation of local wind-waves at Kalpakkam from remote forcing effects of Southern Ocean swells. *Ocean Engineering*, *64*, 23–35.

Remya, P. G., & Kumar, R. (2013). Impact of diurnal variation of winds on coastal waves off South East Coast of India. *International Journal of Ocean and Climate Systems*, *4*(3), 171–179.

Remya, P. G., Kumar, R., Basu, S., & Sarkar, A. (2012). Wave hindcast experiments in the Indian Ocean using MIKE 21 SW model. *Journal of Earth System Science*, *121*(2), 385–392.

Remya, P. G., Vishnu, S., Praveen Kumar, B., Balakrishnan Nair, T. M., & Rohith, B. (2016). Teleconnection between the North Indian Ocean high swell events and meteorological conditions over the Southern Indian Ocean. *Journal of Geophysical Research: Oceans*, *121*, 7476–7494. https://doi.org/10.1002/2016JC011723

Samiksha, S. V., Vethamony, P., Aboobacker, V. M., & Rashmi, R. (2012). Propagation of Atlantic Ocean swells in the north Indian Ocean: A case study. *Natural Hazards and Earth System Sciences*, *12*, 3605–3615.

Semedo, A. (2010). *Atmosphere-ocean interactions in swell dominated wave fields* (pp. 53–54). Uppsala, Stockholm: Uppsala University Press.

Semedo, A., Suseelj, K., & Rutgersson, A. (2009). *Variability of wind sea and swell waves in the North Atlantic based on ERA-40 re-analysis*, Paper presented at Proceedings of the 8th European Wave and Tidal Energy Conference, Uppsala, Sweden.

Semedo, A., Suseelj, K., Rutgersson, A., & Sterl, A. (2011). A global view on the wind sea and swell climate and variability from ERA-40. *Journal of Climate*, *24*, 1464–1479.

Snodgrass, F. E., Groves, G. W., Hasselmann, K. F., Miller, G. R., Munk, W. H., & Powers, W. H. (1966). Propagation of swell across the Pacific. *Philosophical Transactions of the Royal Society London*, *A259*, 431–497.

Wu, L., Rutgersson, A., Sahlée, E., & Guo Larsén, X. (2016). Swell impact on wind stress and atmospheric mixing in a regional coupled atmosphere-wave model. *Journal of Geophysical Research: Oceans*, *121*, 4633–4648. https://doi.org/10.1002/2015JC011576

Zheng, C. W., & Li, C. Y. (2017). Analysis of temporal and spatial characteristics of waves in the Indian Ocean based on ERA-40 wave reanalysis. *Applied Ocean Research*, *63*, 217–228.

Zheng, C. W., Shao, L. T., Shi, W. L., Su, Q., Lin, G., Li, X. Q., & Chen, X. B. (2014). An assessment of global ocean wave energy resources over the last 45 a. *Acta Oceanologica Sinica*, *33*(1), 92–101.

Zheng, C. W., Wang, Q., & Li, C. Y. (2017). An overview of medium- to long-term predictions of global wave energy resources. *Renewable and Sustainable Energy Reviews*, *79*, 1492–1502.